

The Lys 280 → Gln mutation mimicking disease-linked acetylation of Lys 280 in tau extends the structural core of fibrils and modulates their catalytic properties

Harish Kumar¹ | Jayant B. Udgaonkar^{1,2} 

¹National Centre for Biological Sciences, Tata Institute of Fundamental Research, Bengaluru, India

²Indian Institute of Science Education and Research, Pune, India

Correspondence

Jayant B. Udgaonkar, National Centre for Biological Sciences, Tata Institute of Fundamental Research, Bengaluru 560065, India.

Email: jayant@ncbs.res.in; jayant@iiserpune.ac.in

Funding information

Department of Biotechnology, Ministry of Science and Technology; National Centre for Biological Sciences

Abstract

Amyloid fibrillar aggregates isolated from the brains of patients with neurodegenerative diseases invariably have post-translational modifications (PTMs). The roles that PTMs play in modulating the structures and polymorphism of amyloid aggregates, and hence their ability to catalyze the conversion of monomeric protein to their fibrillar structure is, however, poorly understood. This is particularly true in the case of tau aggregates, where specific folds of fibrillar tau have been implicated in specific tauopathies. Several PTMs, including acetylation at Lys 280, increase aggregation of tau in the brain, and increase neurodegeneration. In this study, tau-K18 K280Q, in which the Lys 280 → Gln mutation is used to mimic acetylation at Lys 280, is shown, using HX-MS measurements, to form fibrils with a structural core that is longer than that of tau-K18 fibrils. Measurements of critical concentrations show that the binding affinity of monomeric tau-K18 for its fibrillar counterpart is only marginally more than that of monomeric tau-K18 K280Q for its fibrillar counterpart. Quantitative analysis of the kinetics of seeded aggregation, using a simple Michaelis–Menten-like model, in which the monomer first binds and then undergoes conformational conversion to β -strand, shows that the fibrils of tau-K18 K280Q convert monomeric protein more slowly than do fibrils of tau-K18. In contrast, monomeric tau-K18 K280Q is converted faster to fibrils than is monomeric tau-K18. Thus, the effect of Lys 280 acetylation on tau aggregate propagation in brain cells is expected to depend on the amount of acetylated tau present, and on whether the propagating seed is acetylated at Lys 280 or not.

KEYWORDS

hydrogen-deuterium exchange mass spectrometry, kinetics, neurodegenerative disease, seeding, tau fibrils

1 | INTRODUCTION

Abbreviations: 0N4R, isoform of tau containing four repeats; 2N4R, largest isoform of human tau; AFM, atomic force microscopy; HX, hydrogen exchange; MS, mass spectrometry; ThT, thioflavin T.

The aggregation of specific proteins in the brain has been linked to various neurodegenerative diseases.^{1,2} These

proteins form different types of aggregates, including oligomers and amyloid fibrils, which differ in size and structure, and it has not been easy to link the physical properties of aggregated protein to differing disease pathologies. The molecular mechanisms by which oligomers and/or fibrils cause various neurodegenerative diseases remain to be understood, and the cellular factors regulating this process also need to be identified. It appears that oligomers, which are smaller in size than amyloid fibrils, are toxic to neurons, whereas amyloid fibrils seem to propagate the disease pathology in the brain.^{3–5} It appears that amyloid fibrils can act as infectious particles, and can spread from a donor cell to an acceptor cell via a prion-like mechanism.^{6,7} Several amyloid-forming proteins, including tau, appear to follow a prion-like mechanism for the propagation of aggregate in the brain.^{8,9} However, the molecular parameters governing amyloid fibril formation and thereby determining the extent of pathology are not well understood.

Tau is an intrinsically disordered protein that expresses mainly in the cytosol of neurons of the central nervous system.^{10–12} It functions as a microtubule (MT) binding protein that regulates the dynamics of microtubule assembly.¹³ Various disease-linked mutations and post-translational modifications (PTMs) are known to modulate the binding affinity of tau for microtubules,^{14,15} as well as the pathological aggregation of tau.^{10,12,16} Both gain of pathological function, and loss of physiological function (MT binding) of tau could be associated with neurodegenerative diseases. However, studies carried out with tau-knockout mice did not find any developmental defects.^{17,18} These results suggested that tau is not an essential gene, and that loss of physiological function is not pathological; conversely, it appears that tau gains pathological function in diseases.

Tau aggregates extracted from the brains of patients of different tauopathies, exhibit distinct structural folds and are monomorphic, suggesting that a specific fold is associated with a specific tauopathy.^{19–23} PTMs may play an important role in defining the structural diversity of tau fibril folds (strains) found in the brain,²² and it is expected that *in vitro* studies of tau fibril formation will reveal the mechanisms by which the structural diversity is modulated. Tau aggregates extracted from tauopathy patients were found to be hyperphosphorylated^{24,25} and acetylated.²⁶ Lysine acetylation has been shown to modulate the physiological function as well as the pathological aggregation of tau.²⁶ Various lysine residues including Lys 280, were found to be acetylated in the aggregates extracted from the brain of tauopathy patients.^{22,26} Lys 280 is of particular interest because its acetylation was found to be prominent in aggregates extracted from all 4R tauopathies,²⁶ and its deletion, which is disease-

linked, leads to pathological aggregation of tau.^{27,28} *In vivo* studies using transgenic *Drosophila* expressing the tau-K280Q mutant variant, have found that the mutation leads to fly locomotion defects; however, over-expression of tau-K280Q significantly delays fly death.²⁹ In a recent study,³⁰ transgenic mice expressing tau-K280Q were found to show a reduction in insoluble tau, as well as a reduction in hyperphosphorylation, which appeared to suppress tau pathology. Together, these data suggest that acetylation of Lys 280 might have a protective role in tau-related pathologies.

In contrast, previous *in vitro* studies had found that the K280Q mutation, which mimics Lys 280 acetylation, results in the inhibition of the function of tau, and promotes its aggregation.²⁶ Similar results were observed upon site-specific acetylation of Lys 280 using a protein semisynthesis based methodology.³¹ Obtaining tau protein that is acetylated only at Lys 280 in this way is not easy. Consequently, the tau-K18 K280Q mutant variant has been used as a mimic of tau acetylated only at Lys 280, in many studies of tau aggregation.^{26,29–32} Previous studies of tau possessing this acetylation mimicking mutation have not examined the effect on the seeding of fibril formation, a template-dependent process that is mainly responsible for the prion-like spread of pathological tau aggregates in the brain.

In this study, it was found that the effect of the acetylation of Lys 280 in the 4R tau variant tau-K18, studied in the acetylation mimic tau-K18 K280Q, was to seemingly promote amyloid fibril formation by reducing the lag phase. The acetylation mimic was found to form two types of fibrils differing in their structural cores. One type had a structural core identical to that of tau-K18, while the other type had an extended structural core. The fibrils formed by tau-K18 and tau-K18 K280Q were found to differ in their seeding ability, and the difference in catalytic efficiency could be attributed to the difference in the structural core. Unexpectedly, the fibrils formed by tau-K18 K280Q were found to be less efficient in catalyzing the conversion of monomeric tau into amyloid fibrils. The study describes a detailed kinetic and structural mechanism of how acetylation of Lys 280 might alter the disease-linked catalytic properties of tau aggregates.

2 | RESULTS

2.1 | Tau-K18 K280Q aggregates faster than tau-K18

To study the role of the acetylation of Lys 280 in tau, an acetylation mimic of tau was made by introducing a

single point mutation in tau-K18, which contains four microtubule-binding repeats. Lys 280 was replaced with Gln by site-directed mutagenesis, and the tau-K18 K280Q variant was used as a mimic of tau-K18 acetylated at Lys 280. ThT fluorescence intensity was used to monitor the kinetics of aggregation. Both tau-K18 and tau-K18 K280Q converted into fibrils with typical sigmoidal kinetics (Figure 1a). Tau-K18 converted into fibrils with a lag phase of ~ 7 hr duration, while tau-K18 K280Q converted into fibrils faster than did tau-K18, with a lag phase of ~ 3 hr duration (Figure 1a). The elongation rate constant of tau-K18 K280Q was, however, found to be ~ 1.6 -fold slower than that of tau-K18 (Figure 1a). The ThT fluorescence intensity obtained at saturation of the fibril formation reaction, was ~ 3 -fold higher for tau-K18 K280Q than for tau-K18 indicating that either the fibrils formed by tau-K18 K280Q were structurally different from those formed by tau-K18, or that the amount of the fibrils formed by tau-K18 K280Q was ~ 3 -fold higher than by tau-K18 (Figure 1a). The amount of monomer converted into insoluble fibrils was quantified by measuring the concentration of the remaining soluble tau (see Section 5) at the end of the fibrillation reaction (Figure 1b). In previous studies, the fibrillation of tau was shown to follow a nucleation dependent polymerization model.^{33,34} Hence, the concentration of monomer left in equilibrium with fibrils at the end of the

fibrillation reaction corresponds to the critical concentration, which was slightly higher in the case of tau-K18 K280Q than in the case of tau-K18. Thus, for both tau-K18 and tau-K18 K280Q, similar amounts of monomer had converted into fibrils. Hence, the difference in the ThT fluorescence intensity at saturation of the fibrillation reaction suggested that tau-K18 K280Q forms fibrils that are structurally different from tau-K18 fibrils (Figure 1).

2.2 | Characterization of tau fibrils

To identify the role of the Lys 280 \rightarrow Gln mutation in tau, the morphological properties of the fibrils formed by tau-K18 and tau-K18 K280Q were characterized using atomic force microscopy (AFM) (Figure 2; Figure S1). The AFM images shown in Figure 2 did not reveal the presence of oligomers as a product of aggregation. This was expected: when acetylated at residues K280, K281, and K369, tau-K18 is known to form fibrils and not oligomers.²⁶ In an earlier study of fibril formation by full-length tau, neither the wt protein nor the K280Q mutant variant showed the presence of oligomers along with fibrils at the end of the aggregation reaction.³¹ It has been claimed that tau that had been acetylated only at Lys 280 forms ThS positive oligomers,³¹ but this is unlikely

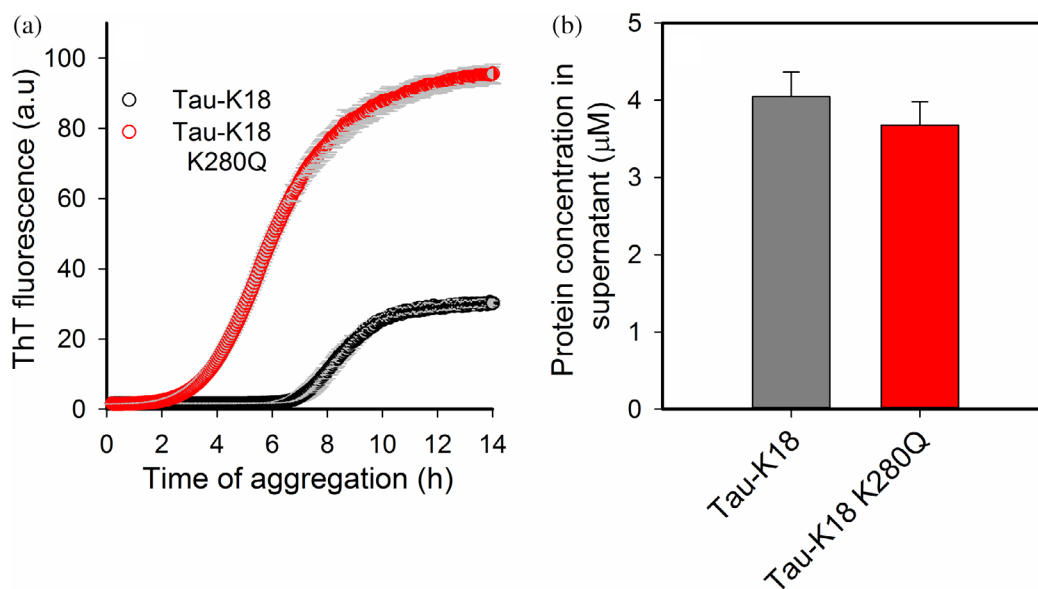


FIGURE 1 Tau-K18 K280Q monomer converts into fibrils faster than tau-K18 monomer. (a) ThT fluorescence-monitored kinetics of aggregate formation by $80 \mu\text{M}$ protein in the presence of $60 \mu\text{M}$ heparin at 25°C , pH 7.3. For tau-K18, the lag time and elongation rate were 7.0 ± 0.3 hr and $0.58 \pm 0.03 \text{ hr}^{-1}$, respectively. For tau-K18 K280Q, the lag time and elongation rate were 3.1 ± 0.2 hr and $0.35 \pm 0.03 \text{ hr}^{-1}$, respectively. The lag time and elongation rate were determined by fitting the data shown in panel a to Equations (4) and (5), respectively, as described in the Experimental Procedures. The error bars in grey in panel a represent the *SD* determined from four repetitions of the aggregation reaction of each protein variant. (b) The concentration of soluble (unaggregated) tau at the end of the aggregation reaction. The error bars represent the *SD* from three independent reactions. ThT, thioflavin T

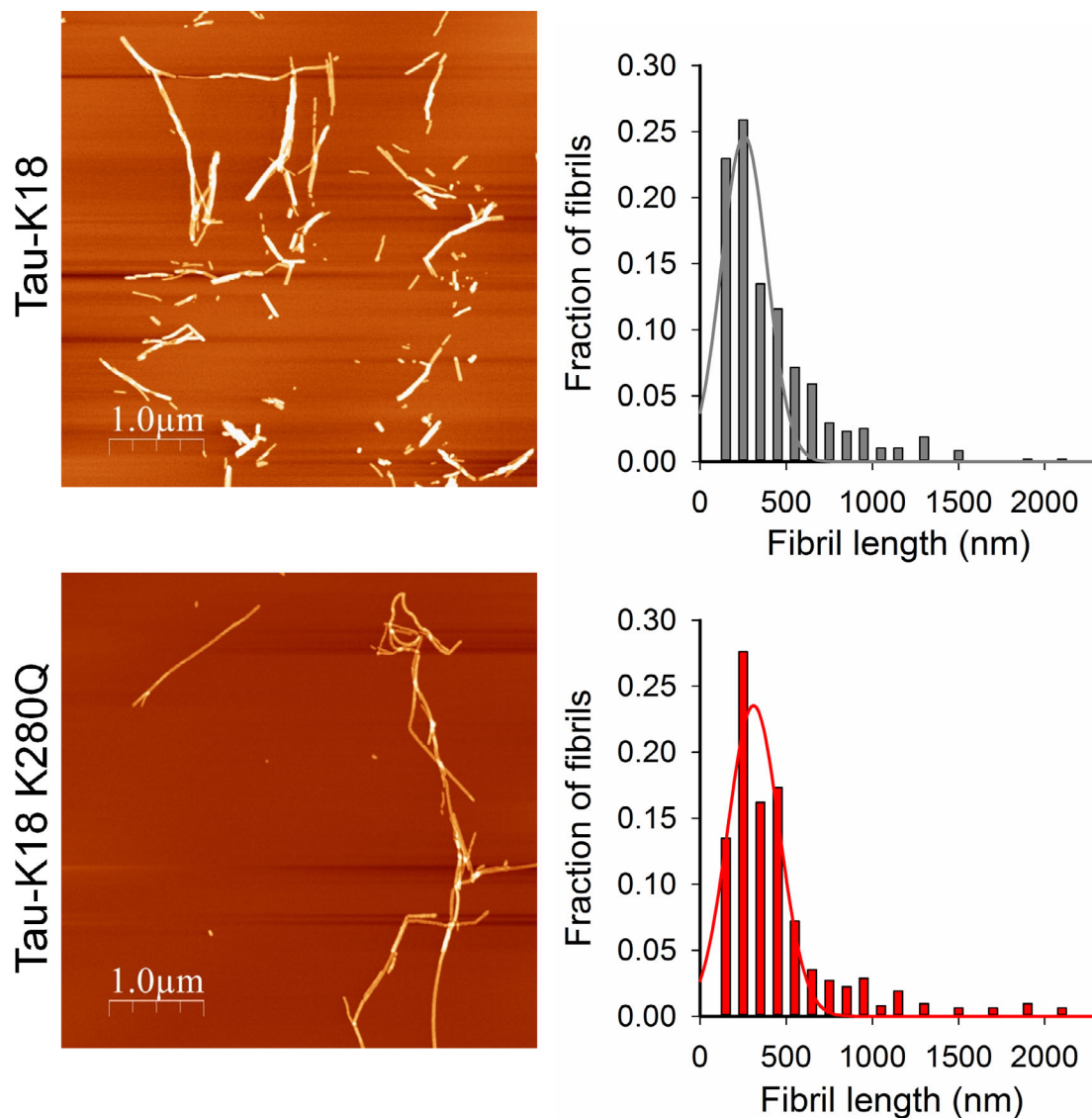


FIGURE 2 Tau-K18 forms shorter fibrils than tau-K18 K280Q. AFM images of fibrils formed by tau-K18 and tau-K18 K280Q at the end of the fibril formation reaction shown in Figure 1a. Fibril length distributions of tau-K18 fibrils and tau-K18 K280Q fibrils at the end of fibril formation reaction. The length distributions were obtained by measuring the lengths of the fibrils from AFM images of fibrils formed in three independent experiments. AFM, atomic force microscopy

because only filaments of tau isolated from diseased brain were found to be acetylated.²⁶ Soluble tau isolated from diseased brain was not acetylated; hence, it is likely that the ThS positive oligomers were fragments that had dissociated from fibrils. In this study, tau-K18 K280Q formed fibrils that were morphologically similar to those formed by tau-K18, but were slightly longer (Figure 2). Tau-K18 fibrils had an average length of ~255 nm, whereas tau-K18 K280Q fibrils were ~310 nm in length. This suggests that tau-K18 K280Q fibrils are more stable than tau-K18 fibrils, and did not therefore fragment into shorter fibrils. This data suggested that the internal structures of the fibrils formed by tau-K18 and tau-K18 K280Q might be different.

2.3 | Structural characterization of fibrils by hydrogen exchange-mass spectrometry (HX-MS)

It was hypothesized that the structural core of tau-K18 K280Q fibrils might be extended and longer than the structural core of tau-K18 fibrils. Due to increased hydrogen bonding in a longer β -sheet, tau-K18 K280Q would be expected to form more stable fibrils (Figure 2). HX-MS was used to identify the difference in the internal structure of the fibrils formed by tau-K18 and tau-K18 K280Q. In HX-MS studies, the amide hydrogen sites that are exposed to the solvent, get labeled by deuterium, and can be assigned to specific segments of the protein sequence,

by carrying out pepsin digestion at low pH under quench conditions (to reduce the back exchange). The peptide map of monomeric tau-K18 was generated as described previously (Figure S2). A 30 s pulse of deuterium label was given by incubating monomeric tau, as well as fibrils of tau-K18 and tau-K18 K280Q, in deuterated buffer at pH 7.3 at 25°C. The percentage of deuterium incorporation in different samples was calculated by running control samples having no deuterium (0% D) and complete deuteration (95% D) (Figure 3). As

expected for an intrinsically unfolded protein, monomeric tau showed complete deuteration in all sequence segments after 30 s of exchange (Figure S3). For tau fibrils, regions that are exposed to the solvent, are highly flexible or which remain unfolded, would get labeled to the same extent as they do in the unfolded monomer (complete deuteration). Regions that are part of the rigid structural core of the fibrils would remain protected, would not be labeled, or would show very little deuterium incorporation.

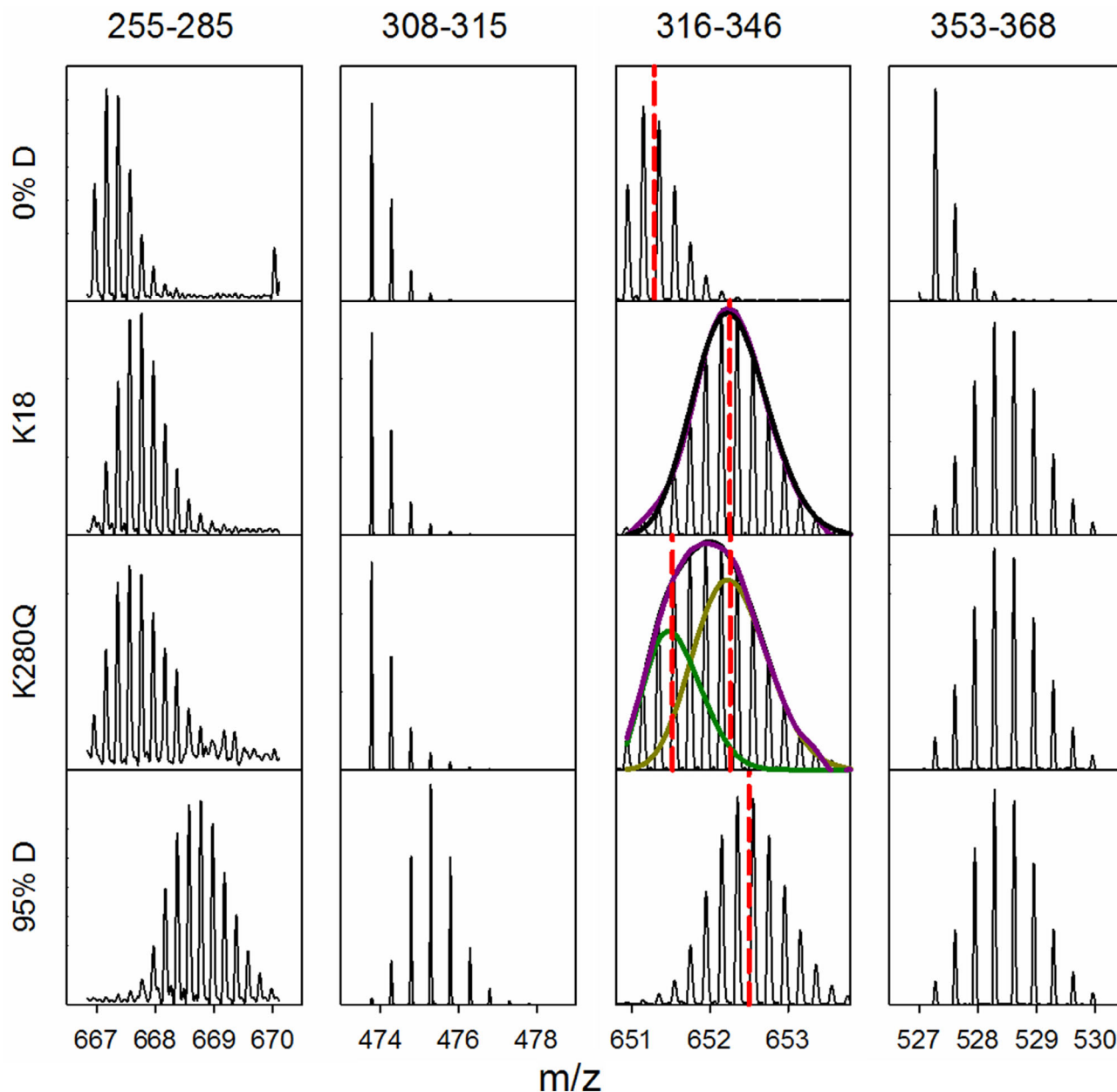


FIGURE 3 Structural heterogeneity in fibrils formed by tau-K18 K280Q. Representative mass spectra, as seen in three independent experiments, of peptide fragments of tau, for fibrils formed by tau-K18 and tau-K18 K280Q, along with the mass spectra of protonated (0% D) and deuterated (95% D) monomeric tau. The peptide fragment corresponding to sequence segment 316–346 shows a bimodal mass distribution for fibrils formed by tau-K18 K280Q, and a unimodal mass distribution for fibrils formed by tau-K18

In both tau-K18 and tau-K18 K280Q fibrils, sequence segments spanning residues 347–368 became fully labeled (>80% D) (Figures 3 and 4), suggesting that this region does not undergo any structural transition during fibrillation, and remains unfolded and flexible in the fibrils. Sequence segments spanning residues 255–315

were found to remain strongly protected in both tau-K18 and tau-K18 K280Q fibrils, indicating that this region undergoes a structural transition from an unfolded to a β -sheet structure. In tau-K18 K280Q fibrils, the sequence segment spanning residues 316–346 showed a bimodal mass distribution, whereas tau-K18 fibrils showed an

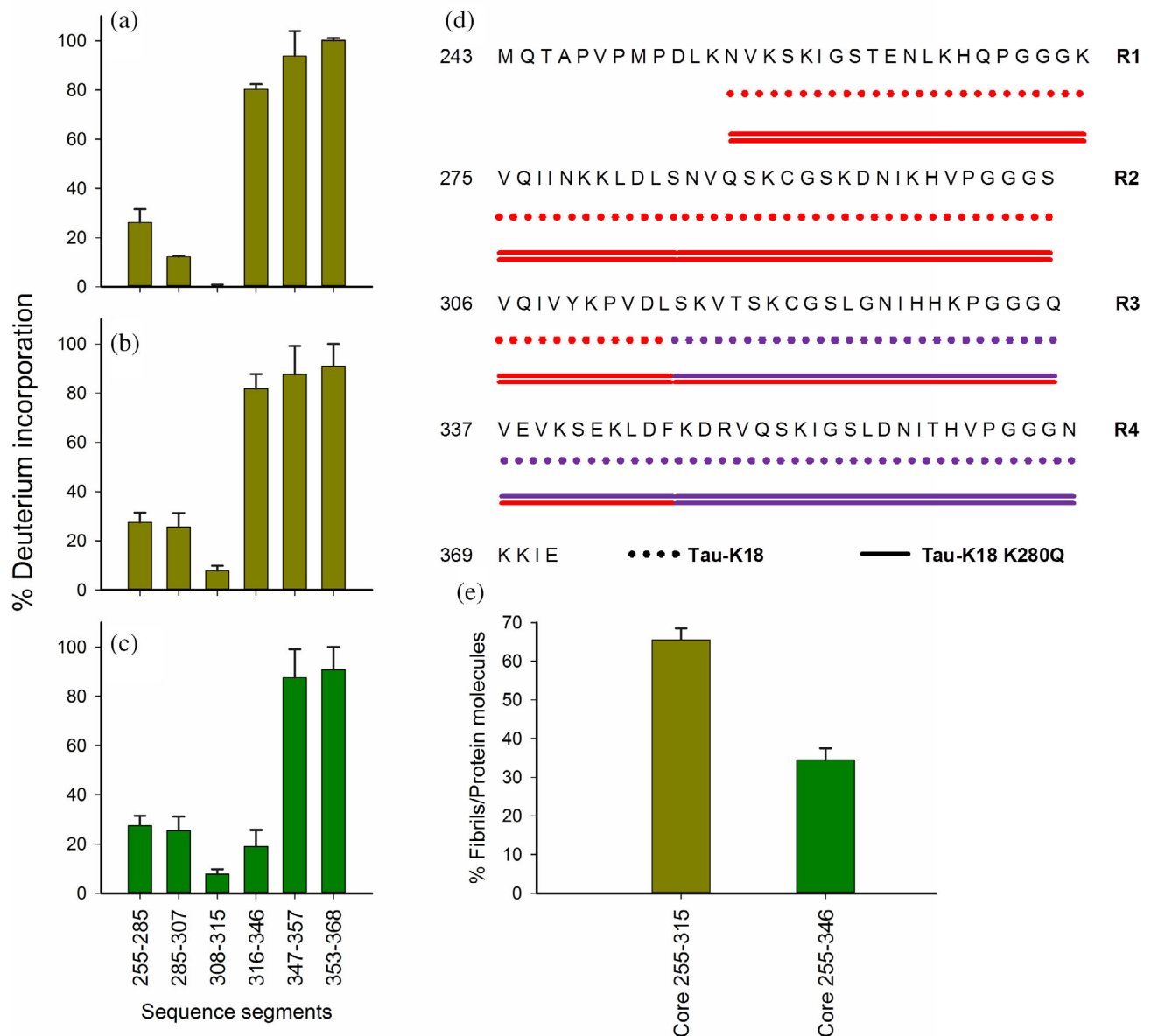


FIGURE 4 The structural core of fibrils formed by tau-K18 and tau-K18 K280Q. The percent deuterium incorporation into different sequence segments of fibrils formed by (a) tau-K18, and (b) and (c) tau-K18 K280Q. The data in panel a correspond to the unimodal mass distributions observed for the sequence segments for fibrils formed by tau-K18. The deuterium incorporation data for sequence segment 316–346 for tau-K18 K280Q in panel b correspond to the higher mass distribution, and in panel c correspond to the lower mass distribution of the observed bimodal distribution. (d) HX protection map of tau-K18 (dotted lines) and tau-K18 K280Q (solid lines). The colors represent the level of deuterium incorporation: (<30% D) strongly protected (red), (>80% D) weakly protected (purple). The two solid lines correspond to data for the two types of fibrils seen for tau-K18 K280Q (panels (b) and (c)). (e) The percentages of protein molecules in tau-K18 K280Q fibrils with and without a structural core extending down to residue 346, were determined from the bimodal mass distribution (by fitting to the sum of two binomial distributions and calculating the area under each peak) seen for sequence segment 316–346 (as shown and described in Figure 3). The error bars represent the *SD* determined from three independent experiments

unprotected unimodal mass distribution (Figure 3). The bimodal mass distribution indicated the presence of two differently protected populations of fibrils, one of which remained unprotected in sequence segment 316–346, as did tau-K18 fibrils, whereas the other was highly protected in this sequence segment.

The relative amounts of the two types of fibrils formed by tau-K18 K280Q were quantified by fitting the bimodal mass distributions to the sum of two binomial distributions, and determining the area under each distribution (Figure 4e). 65% of the fibrils had a structured core spanning residues 255–315, similar to that of tau-K18 fibrils (Figures 3 and 4). 35% of the fibrils had an extended structured core spanning residues 255–346 (Figures 3 and 4). Similar results were obtained when the duration of the deuterium labeling pulse was increased to 300 s (Figure S4). The structural core of the two types of fibrils identified in this study was similar to that of the fibrils formed by 0N4R tau and full-length 2N4R tau in the presence of heparin as determined by SSNMR and cryo-EM, respectively.^{35,36} The 35% of the fibrils that have an extended structural core are expected to have strong intermolecular bonding, and are therefore likely to be more stable and longer. In previous studies, intermolecular forces between β -sheet layers had been shown to determine the length of fibrils.^{37,38} Short amyloid fibrils contain less β -sheet content than long fibrils.³⁷

2.4 | Tau-K18 seed acts as a better catalyst than tau-K18 K280Q seed in catalyzing the seeding reaction

Pathological aggregates of tau are known to spread in the brain by a prion-like mechanism, in which secreted aggregates are taken up by neighboring cells. These aggregates act like catalysts, and convert soluble monomeric protein into aggregates in a template-dependent manner. Hence, factors affecting the fibril elongation rate are expected to alter the prion-like propagation of aggregates. To determine the effect of the Lys 280 \rightarrow Gln mutation on the seeding efficiency of tau seeds, the aggregation of 10 μ M tau-K18 was carried out in the presence of 2% v/v seed (equivalent to \sim 1.6 μ M monomeric protein) made from either tau-K18 or tau-K18 K280Q, at pH 7.3 at 25°C, and the process was monitored by measurement of ThT fluorescence (Figure 5a,b). The final ThT fluorescence intensities were found to be different for the four seeded reactions shown (insets in Figure 5a, b), indicating that the ThT fluorescence intensities per unit mass of fibril were different. To account for this difference, so as to ensure that the kinetic curves truly represent kinetics of formation of new fibrillar mass per unit

time, the kinetic curves shown in the insets of Figure 5a, b were normalized to that obtained when tau-K18 seeds were used with tau-K18 monomer, as described in the Section 5. Tau-K18 seeds were found to catalyze the fibrillation process more rapidly than tau-K18 K280Q seeds, both for tau-K18 monomer (Figure 5a) and for tau-K18 K280Q monomer (Figure 5b). The initial rate of tau-K18 seed elongation was \sim 10-fold higher than that of tau-K18 K280Q seed elongation, when tau-K18 was used as the monomer (Figure 5c), and was \sim 4-fold higher when tau-K18 K280Q was used as the monomer (Figure 5d). This data indicated that tau-K18 seeds were more efficient than tau-K18 K280Q seeds in catalyzing the process of tau fibrillation.

2.5 | Tau-K18 seeds catalyze the conversion of monomer into fibrils faster than tau-K18 K280Q seeds

To understand the mechanism of fibril elongation, and to obtain a quantitative description of the binding of monomer to seeds and their conformational conversion, the aggregation of tau-K18 and tau-K18 K280Q was carried out at different protein concentrations, in the presence of 2% v/v seed (equivalent to \sim 1.6 μ M monomeric protein) (Figure 6). The dependence of the initial rate of fibril elongation on monomer concentration was determined at a constant seed concentration (under pseudo-first-order conditions) (Figure 6). At lower monomer concentrations, the initial rate of fibril elongation was found to depend linearly on monomer concentration. At higher monomer concentrations, the initial rate became independent of monomer concentration, as conformational conversion of monomer to fibrils became the rate-limiting step. This dependence of initial rate on monomer concentration could be described well by a Michaelis-Menten (MM) like model (commonly used for enzyme-catalyzed reactions) in which the monomer acts like a substrate, and the seed plays the role of an enzyme.³⁹ A previous study had been shown that initially during fibril elongation, the number concentration of fibrils remains constant, and that only the length of the fibrils increases.³⁹ Hence, secondary processes do not contribute significantly at the start of seeded fibril formation reaction.³⁹ Modeling the seeding reaction to such a simple model provides a quantitative description of the apparent binding affinity of monomer to seeds (K_m), and the rate constant with which monomer converts into fibrils. These quantitative parameters can be used to compare the properties of the fibrils formed by tau-K18 and tau-K18 K280Q, which could potentially be important in determining their infectivity.

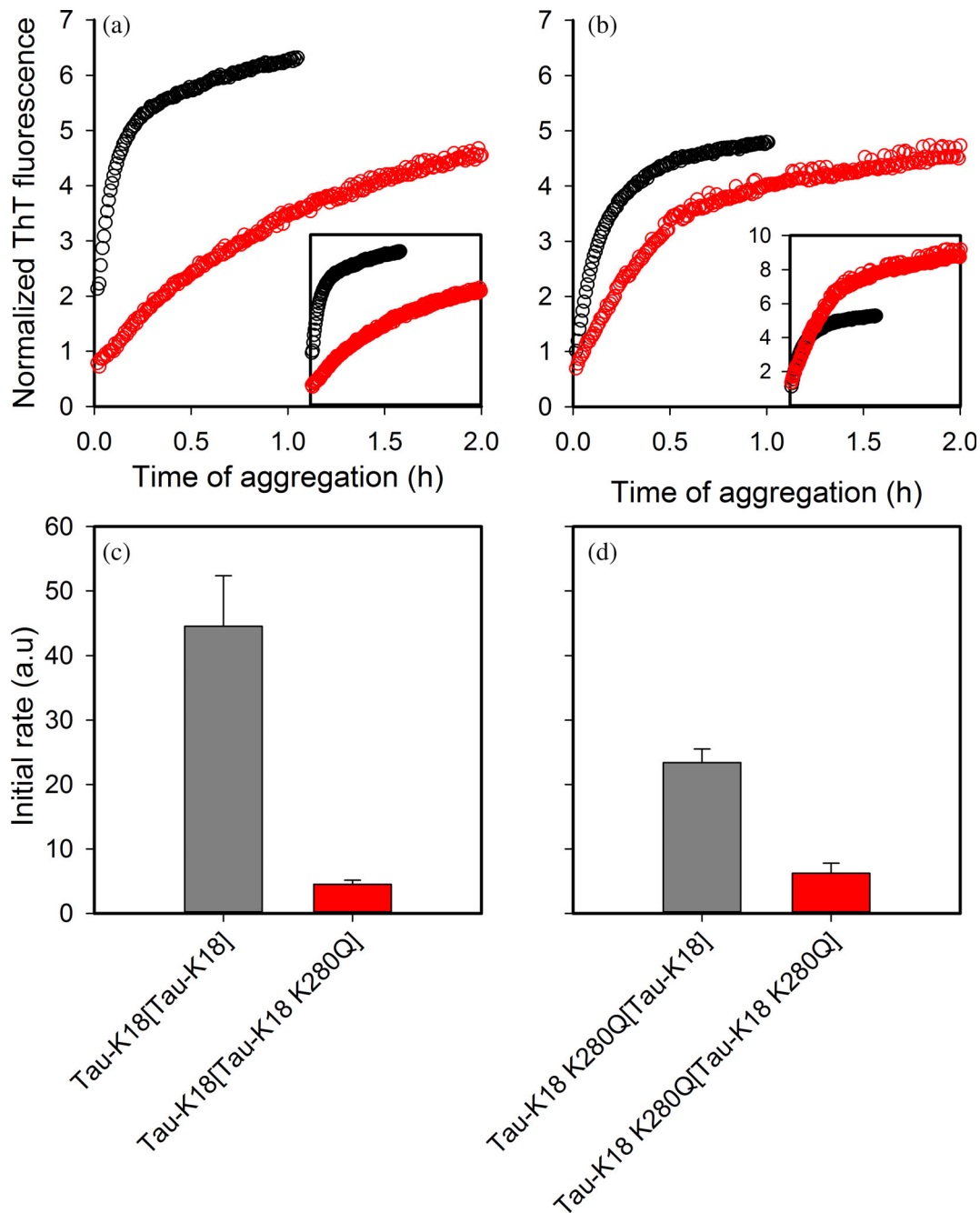


FIGURE 5 Elongation kinetics of tau fibrils: tau-K18 fibrils elongate faster than tau-K18 K280Q fibrils. ThT fluorescence-monitored kinetics of fibril elongation of 10 μM (a) tau-K18, and (b) tau-K18 K280Q monomer in the presence of 2% v/v (equivalent to $\sim 1.6 \mu\text{M}$ monomeric protein) tau-K18 seed (black) and tau-K18 K280Q seed (red). The kinetic curves of aggregation, shown in the insets of panels a and b, have been corrected for the ThT fluorescence intensity contributed by the added seed (see Section 5). These kinetic curves were then normalized to that obtained for tau-K18 monomer with tau-K18 seed, as described in the Section 5, and the normalized kinetic curves are shown in panels (a) and (b). The ThT fluorescence intensity values defining the kinetic curves shown in panels a and b therefore represent the mass of fibrils formed. Initial rate of fibril elongation (obtained by measuring the initial slopes of the kinetic curves shown in panels (a) and (b)) are shown for (c) tau-K18 and (d) tau-K18 K280Q monomer. The nature of the seed is shown inside the square brackets. The error bars in panels (c) and (d) represent the *SD* determined from three independent experiments. ThT, thioflavin T

Before using the MM-like model to determine and compare the catalytic properties of fibril seeds formed from tau-K18 and tau-K18 K280Q, for both seeding and cross-seeding experiments, it was first necessary to

demonstrate that the number concentration of seeds formed from the fibrils of the two proteins were the same. This was done by comparing the lengths, hydrodynamic radii, and molar masses of the seeds formed from the

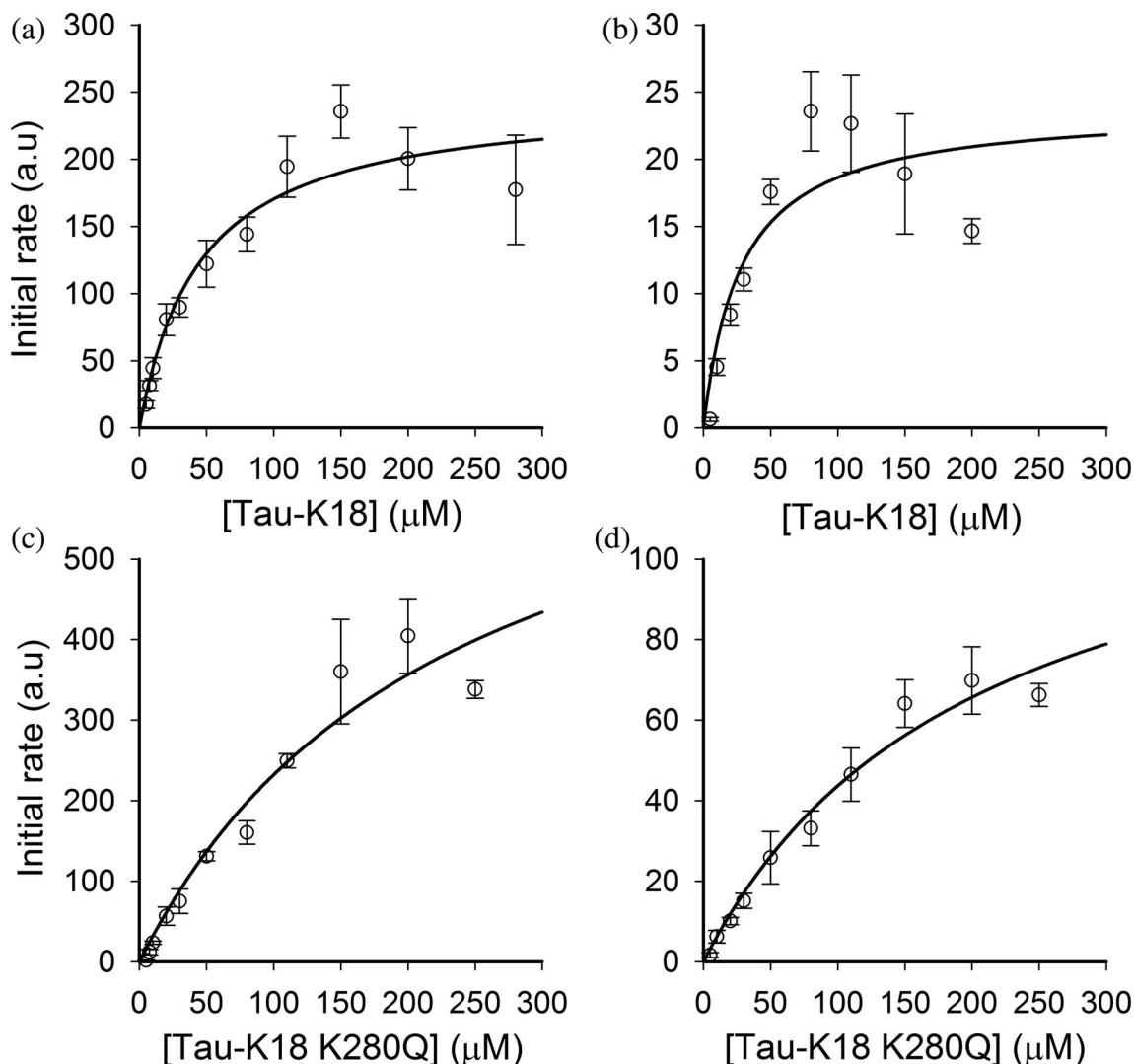


FIGURE 6 Elongation of fibrils follows Michaelis–Menten-like kinetics. Initial rate of fibril formation by monomeric tau-K18 in the presence of 2% v/v (equivalent to ~ 1.6 μM monomeric protein) (a) tau-K18 seed, and (b) tau-K18 K280Q seed versus monomeric tau-K18 concentration. Initial rate of fibril formation by monomeric tau-K18 K280Q in the presence of 2% v/v (equivalent to ~ 1.6 μM monomeric protein) (c) tau-K18 seed, and (d) tau-K18 K280Q seed versus monomeric tau-K18 K280Q concentration. The error bars represent the *SD* determined from three independent experiments

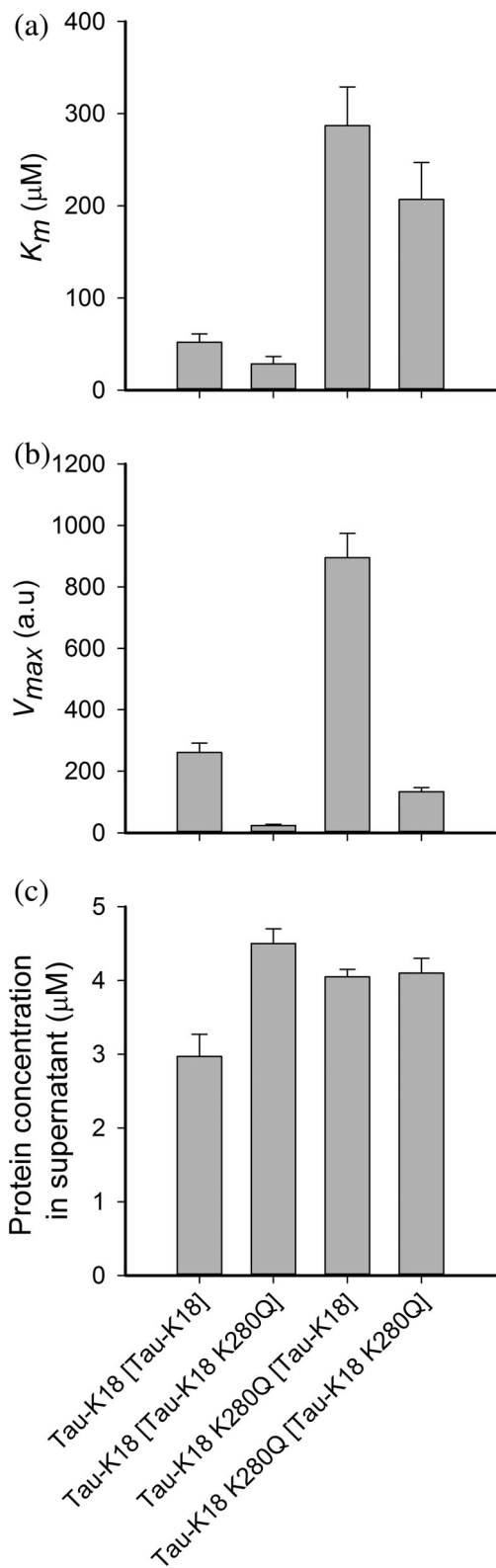
fibrils of 80 μM monomeric tau-K18 and tau-K18 K280Q, using AFM, dynamic light scattering (DLS), and multi angle light scattering (MALS), respectively (Figure S5). Both the AFM and DLS data indicated that the lengths of the seeds were the same for tau-K18 and tau-K18 K280Q, and the MALS data too indicated seeds of very similar average masses (Figure S5). Hence, given that the concentrations of aggregated protein were very similar (Figure 1b), the number concentrations also did not differ significantly.

Tau-K18 seeds were found to bind monomeric tau with a higher K_m value than tau-K18 K280Q seeds (Figure 7a, Table S1). It should be noted that for a MM mechanism, $K_m = \frac{k_{-1} + k_2}{k_1}$ approximates to the binding affinity or dissociation constant $K_d = \frac{k_{-1}}{k_1}$, only if $k_2 \ll k_{-1}$.

This is not true for the catalytic activities of tau-K18 and tau-K18 K280Q: the rate constant of conformational conversion (k_2) effected by tau-K18 seeds was 7 to 10-fold faster than in the case of tau-K18 K280Q seeds. The higher K_m value seen for the binding of tau-K18 seeds to monomeric tau, therefore seems to be only because of the higher catalytic rate constant, k_2 , of the conformational conversion of monomeric tau into fibrils (Figure 7b), when catalyzed by tau-K18 seeds (Figure 7b).

To confirm that this is indeed the case, the critical concentrations for the seeded reactions were determined as the monomer concentrations left in solution after fibril formation was complete (Figure 7c). The critical concentration for such aggregation reactions is equal to the dissociation constant $K_d = \frac{k_{-1}}{k_1}$ for monomer binding to

fibrils.^{40,41} The values of K_d , shown in Figure 7c, were similar for tau-K18 and tau-K18 K280Q, and were more than 10-fold lower than the values of K_m . It is clear that the value of K_m is higher in the case of tau-K18 than tau-K18 K280Q because the value of k_2 is higher.



Since tau-K18 K280Q formed two types of fibrils with different internal structures (Figure 4), it was possible that the ends of the fibrils, which functioned as MM enzymes in aggregation reactions seeded by tau-K18 K280Q fibrils, have different structures and hence, different catalytic properties. When, however, the kinetic data in Figure 6, were fit to a MM model with two classes of catalytic sites (fits not shown), the fits yielded the same value for K_m for both sites, which was the same as the value obtained when the data were fit to the MM model with only one class of catalytic sites (Table S1). Hence, it appears that the two classes of fibrils, although differing in their internal structures, formed seeds of similar apparent binding affinity.

2.6 | Tau-K18 K280Q monomer binds to fibrils with marginally lower affinity than do tau-K18 monomers

The Lys 280 \rightarrow Gln mutation in tau seemed to modulate the structural and functional properties of tau fibrils. However, its influence on the properties of monomeric tau needed to be determined. To understand how the mimicking of the acetylation of Lys 280 affects monomeric tau, the values of K_d for monomeric tau-K18 and tau-K18 K280Q binding to tau-K18 fibrils were determined from measurement of the critical concentrations (Figure 7c, Table S1). It was seen that the critical concentrations, obtained when tau-K18 fibrils were used to seed the fibrillation of monomeric tau-K18 and monomeric tau-K18 K280Q, were the same, and were also the same as the critical concentrations determined for the unseeded fibrillation reactions of the two protein variants

FIGURE 7 Acetylation mimic of Lys 280 modulates the apparent binding affinity of tau monomer to fibrils and catalytic conversion of monomeric protein into fibrils. (a) K_m values for the seeding by different tau fibrils of monomeric tau-K18 and tau-K18 K280Q. (b) Rate of conformational conversion (V_{max}) of monomeric tau-K18 and tau-K18 K280Q into β -sheet fibrils in the presence of different tau fibril seeds. K_m and V_{max} values were obtained by fitting the curves shown in Figure 6 to a simple MM-like model. The error bars represent the SD determined from three independent experiments. (c) The critical concentration was determined as the concentration of soluble (unaggregated) tau remaining at the end of the aggregation reaction of 80 μM tau-K18 and tau-K18 K280Q in the presence of 2% seed. The nature of the seed is shown inside the square brackets. The error bars represent the spread in the data determined from at least two independent experiments. Actual values of K_m , V_{max} and the critical concentration are also listed in Table S1

(Figures 1 and 7c). This was not surprising because the fibrils formed in the tau-K18 seeded reactions had conformationally converted tau-K18 and tau-K18 K280Q at their ends, and monomeric tau-K18 and tau-K18 K280Q were, respectively, binding to these ends.

Also determined, using a MM-like model, were the kinetic parameters governing the seeding of monomeric tau-K18 and tau-K18 K280Q by tau-K18 fibrils (Figure 7a, Table S1). Irrespective of the fibrils used as seeds and of the monomer that was seeded, it was found that the values of K_d were at least 10-fold lower than those of K_m (Figure 7a,c). Hence, in all cases, the higher values seen for K_m were only because of the higher values of k_2 . It was therefore not surprising that the value of K_m correlated so well with that of V_{max} (Figure 7, Table S1) for the different seeding reactions.

2.7 | Structures of cross-seeded fibrils

When the fibrillation of tau-K18 K280Q monomer was initiated using tau-K18 seeds, virtually all fibrils formed had the shorter structural core characteristic of tau-K18 fibrils (Figure 8); the templated fibrils were faithful to the template. Surprisingly, however, when the fibrillation of tau-K18 monomer was initiated using tau-K18 K280Q seeds, few if any fibrils had an extended structural core. This result can be understood by realizing that tau-K18 K280Q seeds consist of both fibrils with a short structural core (65%) and fibrils with an extended structural core (35%). The fibrils formed, with the 35% the extended structural core fibrils acting as the seed, would also be expected to have an extended structural core; nevertheless, such fibrils are not seen (Figure 8). This could only happen if the 65% fibrils with the shorter structural core in the seed, grew much more rapidly upon the addition of tau-K18 monomer, than do the 35% fibrils with the extended structural core. Figure 5 shows that this is indeed the case: the initial rate (Figure 5) as well as V_{max} values (Figure 7b) seen with seeding by tau-K18 fibrils are much faster than those seen with seeding by tau-K18 K280Q fibrils. The fibrils produced from monomeric tau-K18 K280Q upon seeding by tau-K18 K280Q fibrils had a somewhat smaller fraction (25%) of extended structural core fibrils than fibrils produced from tau-K18 K280Q without seeding (Figure 4), again because the shorter core fibrils (tau-K18 like) in the seed grew faster than the extended core fibrils. This effect of self-seeding leading to a reduction of the heterogeneity in fibrillar structure forms the basis of the wide-spread application of multiple cycles of self-seeding to reduce the heterogeneity in fibrils.^{42,43}

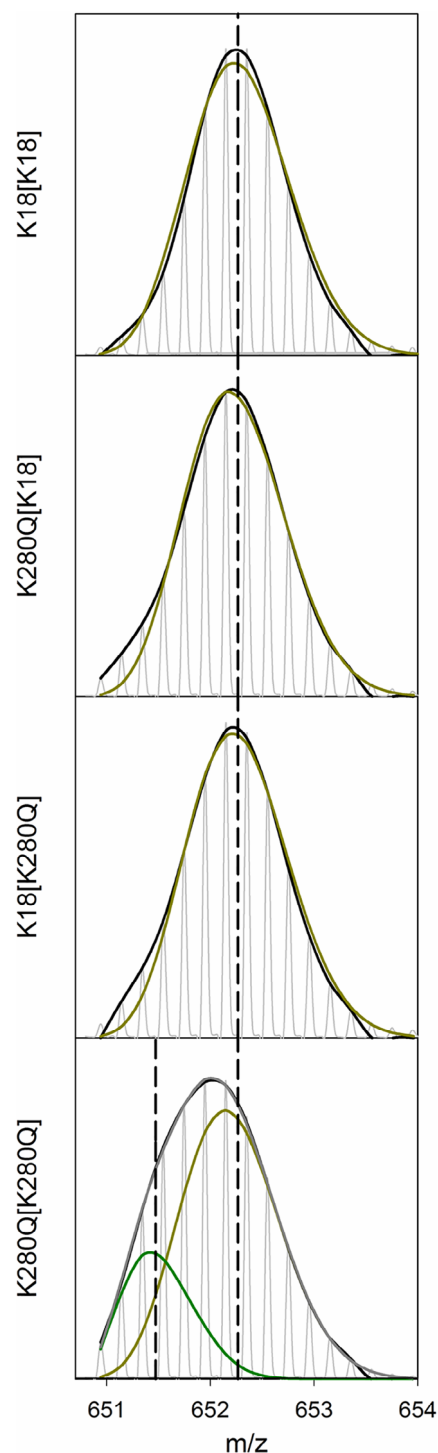


FIGURE 8 Reduction in the structural heterogeneity of fibrils upon seeding. Representative mass spectra, as seen in three independent experiments, of the peptide fragment corresponding to sequence segment 316–346 of tau, for fibrils formed by tau-K18 and tau-K18 K280Q, in the presence of 2% tau-K18 seed and tau-K18 K280Q seed. This peptide fragment shows a bimodal mass distribution, when derived from fibrils formed by tau-K18 K280Q in the presence of tau-K18 K280Q seed, and essentially unimodal mass distributions when derived from fibrils formed by tau-K18 [tau-K18], tau-K18 K280Q[tau-K18] and tau-K18[tau-K18 K280Q]. The nature of the seed is shown inside the square brackets

2.8 | Tau-K18 K280Q monomer converts into fibrils faster than tau-K18 monomer

During fibril elongation, monomeric tau first binds to fibrils, and then conformational conversion (similar to folding) of the intrinsically disordered tau protein into β -sheet-rich fibrils takes place. To determine how the Lys 280 \rightarrow Gln mutation affects the conversion of monomeric tau into fibrils, the fibril elongation rate was monitored at different monomer concentrations in the presence of 2% seed (Figure 6). Figure 7 shows that tau-K18 K280Q monomer converted into fibrils four to fivefold faster than tau-K18 monomer, irrespective of the type of seed used. It was not easy to explain how a single mutation modulates the rate constant of conversion of an IDP to fibrils. It was possible that the mutation might affect the structure of monomeric tau. Although circular dichroism (CD) and DLS measurements showed that tau-K18 and tau-K18 K280Q monomers did not differ in secondary structure or size (Figure S6), it will be important in future studies to determine by the use of a high resolution probe such as NMR, as to whether the two monomeric protein variants are indeed identical in conformation. To further investigate the importance of charge at position 280, the mutant variant tau-K18 K280E was also studied, and the kinetic parameters governing its conversion to fibrils by tau-K18 seed were determined (Figure 9a,c,d). It was found that the values of V_{\max} (and hence that of k_2) for the three protein variants were in the order: tau-K18 K280E > tau-K18 K280Q > tau-K18.

The value of K_d for the binding of tau-K18 K280E to tau-K18 was determined, again from measurement of the critical concentration. It should again be noted that this value of K_d describes the binding of monomeric tau-K18 K280E to conformationally converted tau-K18 K280E at the end of the fibrils. The value of K_d for monomeric tau-K18 K280E was higher than that monomeric tau-K18 K280Q (Figure 9b). Hence, while the values of K_d for the three different charged mutants of monomeric tau to bind to their conformationally converted fibrillar counterparts (grown off tau-K18 seed) were somewhat similar, they increased marginally when the positively charged Lys 280 was replaced with the neutral Gln and then with the negatively charged Glu (Figure 9b).

3 | DISCUSSION

It is well known that PTMs such as acetylation, and phosphorylation can modulate the structural and functional properties of amyloid fibrils.^{22,44,45} For example, phosphorylation of A β 40 leads to the formation of fibrils with an extended structural core, which have better seeding

efficiencies than wt A β 40.⁴⁵ Similarly, acetylated α -synuclein was found to form morphologically and structurally different types of fibrils which had shorter structural core, which are more efficient in seeding activity than is unacetylated α -synuclein.⁴⁴ The finding that tau fibrils from the brains of CBD patients are acetylated and ubiquitinated,²² had suggested that these PTMs could be modulating the fibrillar structure. Indeed, the current study shows that the Lys 280 \rightarrow Gln mutation does modulate the structural core of tau fibrils, which is more extended in tau-K18 K280Q fibrils than in tau-K18 fibrils. This study has then focused on how the Lys 280 \rightarrow Gln mutation made to mimic acetylation at Lys 280 affects the structural mechanism of conformational conversion.

3.1 | Effect of the Lys 280 \rightarrow Gln mutation on the structure of the fibril core

The critical role played by Residue 280, in determining the structural core of tau fibrils, is emphasized by the observation that removal of the charge on it, by the Lys 280 \rightarrow Gln mutation made to mimic acetylation of Lys 280, leads to the formation of two types of fibrils, one type with a structural core spanning residues 255–315, as in the case of tau-K18, and another type with a structural core spanning residues 255–346 (Figure 4). It is perhaps not surprising that a single mutation is so important; it is known, for example, that a single mutation in α -synuclein can lead to the formation of fibrils with different structural folds.^{46,47} Several structures of tau fibrils indicate that Lys 280 forms a salt-bridge with Asp 283 or Asp 314,^{22,35} which would stabilize the fibrils. If the salt bridge with Asp 283, which appears to be present in the structure of fibrils from the brains of CBD patients,²² is formed early during fibrillation, and is important in defining the structural core of the fibrils, then abolishing it, by mutating Lys 280 to Gln, could be responsible for the formation of a different structural fold. The observation that this single mutation can modulate the structural heterogeneity of tau fibrils (Figure 4) is not surprising, as mutations as well as the addition of a small molecule had previously been shown to modulate the structural heterogeneity of α -synuclein fibrils.^{47,48}

3.2 | Catalytic properties of tau fibrils and the role of lysine acetylation

The observation that tau fibrils with a shorter structural core are more efficient in catalyzing the seeding reaction (Figures 5 and 7b) suggests that the length of the amyloid core plays a role in determining the progress of fibril

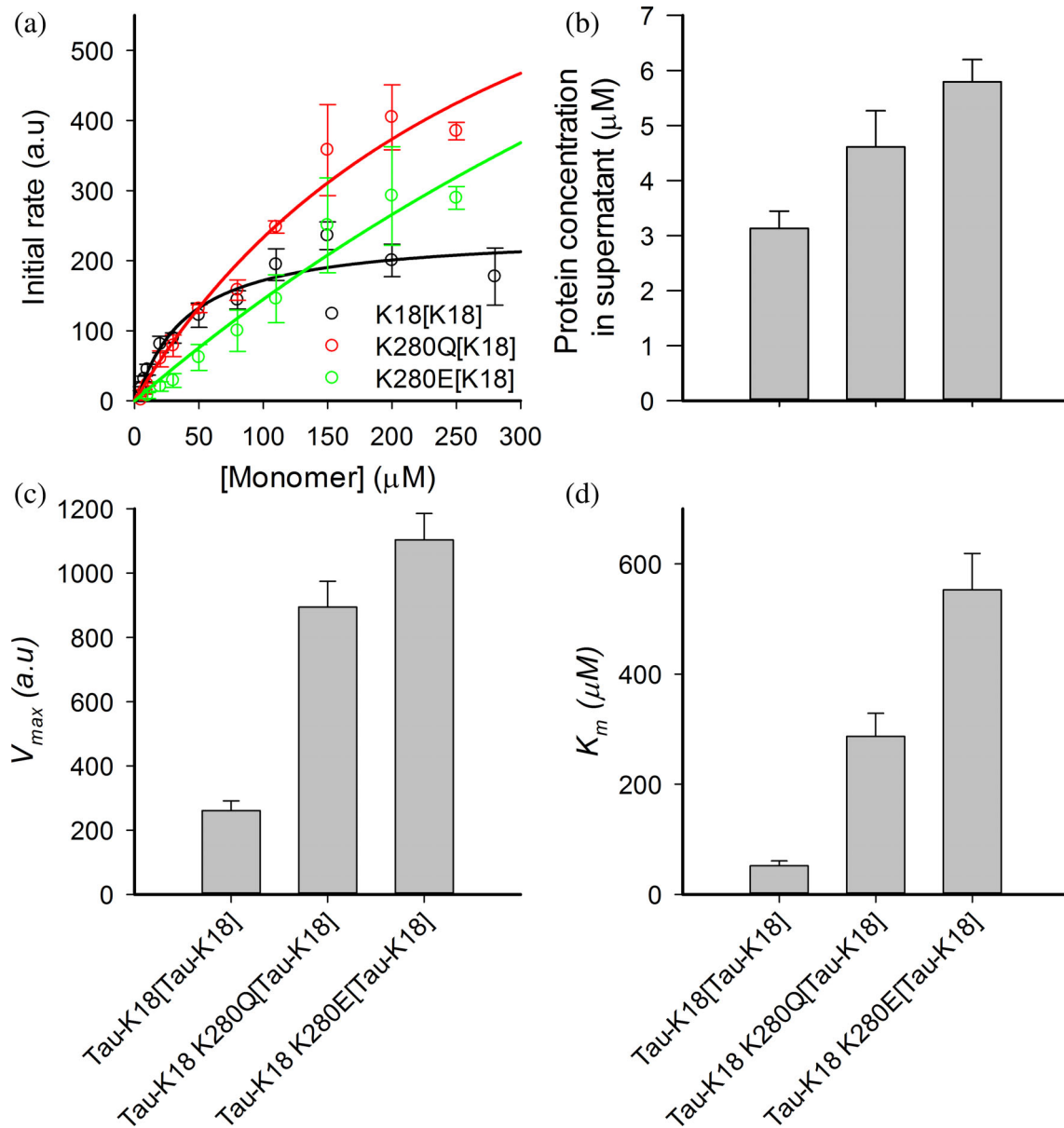


FIGURE 9 Charge on monomeric tau affects its binding affinity to tau fibrils and the elongation rate of fibril formation. (a) Initial rate of fibril formation by different charge mutant variants of monomeric tau in the presence of 2% tau-K18 seed versus monomer concentration. (b) Critical concentrations, or the binding affinities were determined by monitoring the concentration of soluble (unaggregated) protein at the end of the aggregation of 80 μM tau protein in the presence of 2% tau-K18 seed. The error bars represent the SD determined from four independent reactions. (c) V_{max} and (d) K_m values, obtained by fitting the curves shown in panel a to a simple MM-like model, of different charge mutant variants of monomeric tau to tau-K18 seed. The nature of the seed is shown inside the square brackets. The error bars in panels (a), (c), and (d) represent the SD determined from three independent experiments

propagation. A previous study on yeast prion had suggested that the length of the amyloid core determines the infectious nature of distinct prion strains; a strong prion strain had a shorter structured core relative to a weak prion strain.⁴⁹ One goal of the current in vitro study was to explore how acetylation of Lys 280, mimicked here by the Lys 280 \rightarrow Gln mutation, might affect the infectious nature, and thus the spread of tau aggregates in the brain. The two types of tau fibrils found in this study,

might spread differently from cell to cell via a prion-like mechanism. The tau fibril with the higher catalytic efficiency is expected to spread rapidly. Since the tau-K18 K280Q fibrils were 7 to 10-fold less efficient in catalyzing the conversion of monomeric tau into β -sheet fibrils (Figure 7b), spreading could be expected to be 7 to 10-fold less efficient, and a larger number of aggregates would be required to spread the pathology efficiently. On the other hand, monomeric tau-K18 K280Q converts into

fibrils four to fivefold faster than monomeric tau-K18 does (Figure 7b); hence, propagation can be expected to be four to fivefold more efficient, with a shorter incubation period, or with a smaller number of aggregates being required to spread the pathology. It seems that the net effect of acetylation of Lys 280 on disease propagation in the brain will depend on the concentration of acetylated versus unacetylated tau, and on whether the propagating seed is acetylated or not. It should be noted that the difference in the conversion rate of monomeric protein cannot be attributed to any difference in the structure and size of tau-18 and tau-K18 K280Q, as these do not appear to differ significantly (Figure S6).

A major result of the current study is that the charge at position 280 plays an important role in the stabilization of the transition state of the folding reaction leading to the conversion of the template-bound disordered tau conformation to a β -sheet conformation. It is known that aggregation rates correlate well with β -sheet propensity,⁵⁰ but Lys, Gln and Glu do not differ significantly in this property. The aggregation rate also correlates negatively with the net charge on the protein, and the Lys 280 \rightarrow Gln and Lys 280 \rightarrow Glu mutations do reduce the net positive charge that tau has at physiological pH. It is, however, unlikely, that the effect of the mutations is the outcome of their reducing the net positive charge, because the aggregation has been induced by heparin, which itself would have greatly reduced the net charge positive charge on tau.⁵¹

One explanation for the observed slower conversion rate for tau-K18, could be that the transition state for the folding (conversion) reaction involves a positive charge in the vicinity of residue position 280, which is destabilized when Lys is present at position 280 and stabilized when Glu is present. Another explanation could be that, due to the formation of a salt-bridge by Lys 280 in the monomeric protein, it might adopt a compact conformation that shields the amyloid forming motif, VQIINK. In fact, a previous study has shown that various diseases-linked mutations in tau promote its aggregation by disrupting local structure in the monomeric protein, leading to the exposure of VQIVYK.⁵¹ If the monomeric protein retains its compact conformation upon binding to the fibril end, its conversion to the fibrillar conformation would be slow. Mutations abolishing this salt-bridge would disrupt the compact conformation, which would then convert rapidly into a fibrillar conformation. In this context, a molecular dynamic simulation study had shown previously that a Lys 280 deletion mutant variant forms extended conformations due to lack of the salt-bridge and hydrogen bonds.⁵² The extended conformations were found to aggregate faster than compact conformations.⁵² The Lys 280 \rightarrow Gln mutation, is also likely to lead to the adoption of extended conformations, which

expose amyloid forming motifs and thus enable rapid conformational conversion.

3.3 | Origin of structural heterogeneity during the course of fibril formation

Fibril formation by tau follows a nucleation dependent polymerization (NDP) mechanism, in which nucleus formation is the rate-limiting step.^{33,34} In a NDP mechanism, it is possible that multiple nucleation events take place simultaneously, and differently structured nuclei convert into structurally different fibrils. Differentially altering the stability of early aggregates formed on different aggregation pathways can be expected to result in a change in the structural heterogeneity of fibrils. The observation that the Lys 280 \rightarrow Gln mutation accelerates nucleation (Figure 1) indicates that it might favor the formation of specific early aggregates by stabilizing them. In previous studies, lysine acetylation was also shown to induce the aggregation of tau,^{26,31} but the mechanism by which it promotes aggregation was not understood. It is possible that it reduces the barrier height of nucleation by altering electrostatic interactions. A previous study using a single molecule technique found that deletion of Lys 280 increased the nucleation rate, and leads to the rapid formation of oligomers during early stages of aggregation due to reduced electrostatic repulsion between monomers.⁵³

The observation that only 35% of the heterogeneous fibrils formed by tau-K18 K280Q had an extended structural core (Figure 4) implies that the extended structural core fibrils elongate slower than the shorter core fibrils. In fact, tau-K18 fibrils, which have the shorter structural core, were found to elongate faster than tau-K18 K280Q fibrils (Figure 5 and 7b). Furthermore, fibrillation of tau-K18 in the presence of tau-K18 K280Q seed (containing 35% fibrils with an extended structural core) leads to the formation of fibrils with the shorter structural core (Figure 8), which is only possible if fibrils with the shorter core elongate more rapidly than do the extended core fibrils. The observation that the fibrillation of tau-K18 K280Q has a shorter lag phase compared to that of tau-K18 (Figure 1) suggests that the fibril with a higher stability and extended structural core nucleates more rapidly but elongates slowly, whereas the fibril with the shorter structural core nucleates slowly but elongates more rapidly.

3.4 | Determination of the structural core of the fibrils by HX-MS

In this study, HX-MS measurements have shown that the microtubule binding repeats (MTBRs) R2 and R3 are part

of the structural core, because their sequence segments were found to be very strongly protected against HX. In the case of aggregates isolated from the brains of CBD patients, which are formed by the 4R tau isoform (like tau-K18), cryo-EM studies^{21,22} have shown that the structural core spans R2, R3, and R4. It is possible that R4 is part of the structural core of fibrils formed by tau-K18 *in vitro*, but because it is dynamic, as has been shown in the case of fibrils formed by full-length tau,³⁶ it shows weak protection against HX. HX would then not pick it up as being part of the structural core. This is likely to be so, because in the case of tau-K18 K280Q, at least part of R4 has gained sufficient protection, and can hence be identified as being part of the structural core. It is important to remember that tau-K18 spans residues 244–372 of tau, and thus has only four residues beyond the end of R4. Since the structural core of tau can extend up to residue 380,^{21,22} it is possible that it appears to be shorter in this study because of the missing eight residues.

The observation that the binding affinity of monomer to fibril decreases, albeit to a small extent, when Lys 280 is replaced by Gln, and decreases further, again slightly, when Lys 280 is replaced by Glu (Figure 9) provides a clue about the structures of the fibrils formed by tau-K18 and tau-K18 K280Q. Fibrils isolated from the brains of CBD patients, which contain only 4R tau (contains all four MTBRs), have Lys 280 facing toward the outside from the structural core, and appearing to form a salt-bridge with Glu 283.²² The position of this salt-bridge is such that its presence or absence would be expected to affect the binding affinity of monomeric tau to the fibril end to only a small extent, as is observed in this study. Thus, it is likely that the structure of fibrils, studied here, is similar to the structure of the fibrils isolated from the brains of CBD patients.

4 | CONCLUSION

In this study, the use of the tau-K18 K280Q variant as an acetylation mimic, has shown that acetylation of Lys 280 could lead to the formation of fibrils with an extended structural core, compared to the shorter structural core seen in the case of tau-K18. Fibrils of tau-K18 K280Q convert monomeric tau into fibrils more slowly than do fibrils of tau-K18. This result suggests a protective role for Lys 280 acetylation. In contrast, monomeric tau-K18 K280Q is converted more rapidly into fibrils than is monomeric tau-K18. These results suggest that the net effect of the acetylation of Lys 280 in brain cells could be pathogenic or protective, depending on the amount of acetylated tau present, and on whether the propagating seed is acetylated at Lys 280 or not. The current study

provides an insight into how structurally different folds of amyloid catalyze the conversion of monomeric protein into fibrils.

5 | MATERIALS AND METHODS

5.1 | Protein expression and purification

The plasmid pET22b containing the human tau-K18 gene, generated from pET4RPH, a kind gift from Prof. Takashi Konno, was modified using site-directed mutagenesis. Two native cysteines were replaced with serines, and Lys 280 was mutated to either Gln or Glu in the mutant variants, tau-K18 K280Q and tau-K18 K280E, respectively. For fluorescence studies, a single cysteine (I354C) or tryptophan (I354W) was introduced. The fragment of tau (UniProtKB—P10636) which contains four microtubule-binding repeats (tau-K18) was prepared as described previously.³⁹ The purity of each protein was checked using SDS-PAGE and electrospray ionization mass spectrometry, and no contaminated protein was observed. Purified protein was flash-frozen in liquid N₂, and stored at –80°C. The concentration of protein in solution was determined using the BCA (Thermo Scientific) assay, for which bovine serum albumin was used as the standard, with the background signal of the buffer (sample without protein) being subtracted.

5.2 | Chemicals, buffers and aggregation conditions

Reagents used for experiments were of the highest purity grade available from Sigma Aldrich, unless specified otherwise. GdnHCl was procured from USB (USA), and formic acid from Merck. Tau fragment which contains four microtubule-binding repeats from residues 244 to 372 of the full-length human tau was used in this study. Aggregation was carried out by incubating 80 μM tau protein in aggregation buffer (25 mM Tris–HCl buffer, 150 mM NaCl, pH 7.3) at 25°C. The aggregation reaction was initiated by the addition of heparin (molecular mass ~12 kDa, Himedia Laboratories) at a heparin to protein concentration ratio of 3:4.

5.3 | Monitoring the process of aggregate formation using ThT fluorescence

The aggregation reaction of tau was carried out in a 96 well plate at 25°C in a Fluoroskan instrument (Thermo Scientific) in the presence of 32 μM ThT. The

kinetics of aggregate formation was monitored by measuring the ThT fluorescence emission at 475 nm upon excitation at 440 nm.

Formation of fibril seed and seeding: 80 μ M protein was aggregated as described above. At a time corresponding to $3 \times t_{50}$, (t_{50} was the time at which the fluorescence intensity reached 50% of its final value), the aggregated protein solution was centrifuged at 20,000g for 30 min at 15°C. The pellet containing the aggregated protein was resuspended in aggregation buffer, and sonicated as described previously.³⁹ This sonicated solution was used to seed a fresh aggregation reaction in the presence of heparin. All the seeding reactions were carried out using a fixed concentration of seed (2% v/v from the 80 μ M aggregated protein, which was equivalent to \sim 1.6 μ M monomeric protein). The ThT fluorescence intensity of the seed was subtracted from the ThT fluorescence intensities measured during the seeded aggregation reaction so that the ThT fluorescence intensity at any time was a direct measure of the amount of new fibrils formed at that time.

Fibril seeds produced from fibrils formed in the presence of ThT were used because it could then be confirmed that the kinetics of formation of the fibrils, as well as their final ThT fluorescence intensity, were the same for multiple batches of seed production. These were important criteria for ensuring that the seeds produced in successive batches were similar to each other. It is important to note that a previous study had shown that the presence of ThT does not affect the kinetics of tau aggregation.³⁹ Moreover, in this study, fibril seeds produced from fibrils formed in the presence of ThT were shown to have the same activity as fibril seeds produced from fibrils formed in the absence of ThT (Figure S7). Thus, ThT does not interfere with the seeding activity.

Five types of seeded aggregation reactions were carried out: tau-K18 monomer with tau-K18 seeds (tau-K18 [tau-K18]), tau-K18 monomer with tau-K18 K280Q seeds (tau-K18[tau-K18 K280Q]) tau-K18 K280Q monomer with tau-K18 K280Q seeds (tau-K18 K280Q[tau-K18 K280Q]), tau-K18 K280Q monomer with tau-K18 seeds (tau-K18 K280Q[tau-K18]), and tau-K18 K280E monomer with tau-K18 seeds (tau-K18 K280E[tau-K18]). The final corrected (see above) ThT fluorescence intensity was found to be different in each case, even when the same amount of different monomer was aggregated. To properly compare the kinetics of the seeded reactions to each other, it was therefore necessary to normalize the kinetic curves of the different seeded reactions to other.

The kinetic curves for tau-K18 K280Q[tau-K18 K280Q], tau-K18[tau-K18 K280Q], tau-K18 K280Q[tau-K18], and tau-K18 K280E[tau-K18] were normalized to that of tau-K18[tau-K18] in the following manner. For

each kinetic curve, the final ThT fluorescence intensity was determined at the end of the aggregation reaction. At each monomer concentration, c , the ThT fluorescence intensity corresponded to that of a concentration c_{crc} of fibril, where c_{crc} was the critical concentration (see below), and the ThT fluorescence intensity per unit fibril concentration was then determined. Then, the ratio of this quantity for the seeded reaction (tau-K18 K280Q[tau-K18 K280Q], tau-K18[tau-K18 K280Q], tau-K18 K280Q [tau-K18], or tau-K18 K280E[tau-K18]) to that for tau-K18[tau-K18] was determined, for that monomer concentration. Then, all ThT fluorescence intensity values defining each of the four kinetic curves obtained at the same monomer concentration were divided by this ratio.

5.4 | Determination of critical concentration

At the end of the aggregation reaction, the aggregated protein solution was centrifuged at 70,000g for 60 min at 25°C to remove the aggregated protein from the samples. Light scattering experiments indicated that the supernatant did not contain any residual aggregate. The efficacy of the centrifugation step was confirmed by carrying out the centrifugation for 30, 60, and 120 min. The concentration of tau in the supernatant was found to be the same, confirming that centrifugation at 70,000g for 60 min efficiently removed all aggregated protein. The concentration of monomeric protein in the supernatant was determined by measurement of its Tyr fluorescence at 305 nm, upon excitation at 280 nm, using a FluoroMax-4 (Jobin Yvon Horiba) spectrofluorometer. The Tyr fluorescence of a tau solution of known concentration, as determined by the BCA assay, was used as the standard. It should be noted that SDS-PAGE showed that the protein present in the supernatant was tau-K18 and not an impurity (data not shown). Moreover, the protein in the supernatant was aggregation-competent: upon concentration using a 3 kDa Centricon (Merck Millipore), it was found to aggregate.

5.5 | Atomic force microscopy (AFM)

AFM samples were prepared as described previously.³⁹ The AFM images were acquired in the tapping mode (air), on a Bruker Dimension FastScan Bio (Bruker Inc.) instrument. The AFM images were analyzed using the WSxM software.⁵⁴ Length distributions of fibrils was made by measuring the lengths of the \sim 550 \pm 70 fibrils from \sim 18 AFM images from three independent experiments, using the WSxM software.

5.6 | Peptide mapping and hydrogen-exchange mass spectrometry (HX-MS)

The peptide map of tau-K18 was generated as described previously, using the Protein Lynx Global Server (PLGS) software (Waters), and by manual inspection.³⁹ Peptides were generated by carrying out on-line pepsin digestion of the protein. The peptides detected by a Synapt G2 mass spectrometer (Waters) were identified and confirmed by sequencing using the MS/tandem MS (MS^E) method.

HX-MS measurements were carried out as described previously.³⁹ Tau fibrils were spun down for 30 min at 20,000 g. Five microliters of fibrils were added into 95 μ l aggregation buffer made in D₂O to initiate the labeling. The sample was incubated at 25°C for 30 s or for 300 s. After the labeling pulse, the fibrils were dissociated and dissolved within 1 min on ice under quenching conditions (0.1 M Glycine-HCl, 8.1 M GdnHCl, pH 2.5). After desalting under quench conditions using a desalting column, the samples were injected into the HDX module (nanoAcquity UPLC, Waters) coupled to a Synapt G2 mass spectrometer (Waters).

Peptides with their specific retention times and m/z values, were identified using the PLGS software. The percent deuterium incorporation was determined using the Mass Lynx software and HXexpress2.⁵⁵ For each peptide, the percent deuterium incorporation, % D was determined using the following equation:

$$\%D = \frac{(m(f) - m(0\%))}{(m(95\%) - m(0\%))} \times 100 \quad (1)$$

where m(f) is the peptide mass of the fibril, m(0%) is the measured mass of an undeuterated reference sample, and m(95%) is the measured mass of a fully deuterated reference sample.⁵⁶

5.7 | Far-UV circular dichroism (CD)

Far-UV CD spectra were acquired for 15 μ M protein in a 1 mm cuvette using a Jasco J-815 spectropolarimeter. Far-UV CD spectra were acquired at a scan speed of 50 nm/min, at a 1 nm bandwidth with a digital integration time of 2 s at 25°C. Twenty wavelength scans were averaged for each spectrum.

5.8 | Multi angle light scattering (MALS) and dynamic light scattering (DLS)

Fibrils formed by 80 μ M tau-K18 and tau-K18 K280Q were used to make the seeds, and DLS and MALS

measurements were used to determine the hydrodynamic radii (R_H) and molar masses of equal amounts (2%) of the seeds. MALS and DLS experiments were carried out for ~1.6 μ M protein using a Dynapro-99 (Protein Solutions Ltd.) and a Dawn 8+, eight-angle light scattering instrument (Wyatt Technology Corp., Santa Barbara, CA) in batch mode, respectively. To determine the molar masses of the seeds, samples were injected manually at a constant flow rate using a syringe pump into the flow cell. Scattering intensities at multiple angles were measured simultaneously, and the weight average molar masses were determined from Debye plots. Monomeric BSA was used as a reference to normalize the scattering data.

5.9 | Data analysis

The kinetic data obtained for seeded fibril formation reactions were found to be describable by the following Michaelis–Menten like mechanism.³⁹

The values of the kinetic parameters K_m and V_{max} were obtained by fitting the dependence of the initial rate on monomer concentration to the following equation:

$$v = \frac{V_{max}[\text{Monomer}]}{K_m + [\text{Monomer}]} \quad (3)$$

where $K_m = (k_{-1} + k_2)/k_1$, $V_{max} = k_2 [\text{Fibril}_{(n-1)}]$, k_1 , and k_{-1} are the association and dissociation rate constants, respectively, of monomer binding to seed. k_2 is a rate constant for the conformational conversion of monomer into fibril form. When $k_{-1} \gg k_2$, then $K_m = K_D$, the dissociation constant of the Fibril.Monomer complex.

The lag time for naive fibril formation reactions were determined by fitting the kinetic curve to the following equation:

$$S = S_0 + \frac{S_\infty - S_0}{1 + e^{-\left(\frac{t-t_{50}}{\tau}\right)}} \quad (4)$$

where S , S_0 , and S_∞ are the ThT fluorescence intensities at time t , zero, and ∞ , respectively. t_{50} is the time at which the fluorescence intensity is 50%, and τ is a time constant. The lag time (t_{lag}) was calculated as $t_{lag} = t_{50} - 2\tau$ as described previously.³⁴

The elongation rate constant for naive fibril formation reactions were determined by fitting the kinetic curve, after excluding the initial 20% of the curve, to the following single exponential equation:

$$S = S_0 + a \left[1 - e^{-\left(\frac{t}{\tau_{el}}\right)} \right] \quad (5)$$

where a is the signal amplitude, and τ_{el} is the time constant of elongation.

ACKNOWLEDGMENTS

We thank members of our laboratory, Jogender Singh, and Shachi Gosavi, for discussion. The AFM images were collected at the Central Imaging and Flow Facility of the National Centre for Biological Sciences and AFM facility of the Indian Institute of Science Education and Research Pune. J.B.U. is a recipient of a JC Bose National Fellowship from the Government of India. This work was funded by the Tata Institute of Fundamental Research, and by the Department of Biotechnology, Government of India.


AUTHOR CONTRIBUTIONS

Harish Kumar: Conceptualization; data curation; formal analysis; writing-original draft; writing-review and editing. **Jayant Udgaonkar:** Conceptualization; formal analysis; funding acquisition; investigation; resources; supervision; writing-original draft; writing-review and editing.

CONFLICT OF INTEREST

The authors declare no potential conflict of interest.

ORCID

Jayant B. Udgaonkar  <https://orcid.org/0000-0002-7005-224X>

REFERENCES

- Ross CA, Poirier MA. Protein aggregation and neurodegenerative disease. *Nat Med*. 2004;10:S10–S17.
- Chiti F, Dobson CM. Protein misfolding, amyloid formation, and human disease: A summary of progress over the last decade. *Annu Rev Biochem*. 2017;86:27–68.
- Bieschke J, Weber P, Sarafoff N, Beekes M, Giese A, Kretzschmar H. Autocatalytic self-propagation of misfolded prion protein. *Proc Natl Acad Sci U S A*. 2004;101:12207–12211.
- Tanaka M, Komi Y. Layers of structure and function in protein aggregation. *Nat Chem Biol*. 2015;11:373–377.
- Kumar S, Udgaonkar JB. Mechanisms of amyloid fibril formation by proteins. *Curr Sci*. 2010;98:639–656.
- Collinge J, Clarke AR. A general model of prion strains and their pathogenicity. *Science*. 2007;318:930–936.
- Marciniuk K, Taschuk R, Napper S. Evidence for prion-like mechanisms in several neurodegenerative diseases: Potential implications for immunotherapy. *Clin Dev Immunol*. 2013;2013:473706.
- Clavaguera F, Bolmont T, Crowther RA, et al. Transmission and spreading of tauopathy in transgenic mouse brain. *Nat Cell Biol*. 2009;11:909–913.
- Goedert M. Neurodegeneration. Alzheimer's and Parkinson's diseases: The prion concept in relation to assembled A β , tau, and α -synuclein. *Science*. 2015;349:1255555.
- Goedert M, Spillantini MG, Jakes R, Rutherford D, Crowther RA. Multiple isoforms of human microtubule-associated protein tau: Sequences and localization in neurofibrillary tangles of Alzheimer's disease. *Neuron*. 1989;3:519–526.
- Couchie D, Mavilia C, Georgieff IS, Liem RK, Shelanski ML, Nunez J. Primary structure of high molecular weight tau present in the peripheral nervous system. *Proc Natl Acad Sci U S A*. 1992;89:4378–4381.
- Garcia ML, Cleveland DW. Going new places using an old MAP: Tau, microtubules and human neurodegenerative disease. *Curr Opin Cell Biol*. 2001;13:41–48.
- Weingarten MD, Lockwood AH, Hwo SY, Kirschner MW. A protein factor essential for microtubule assembly. *Proc Natl Acad Sci U S A*. 1975;72:1858–1862.
- Guo T, Noble W, Hanger DP. Roles of tau protein in health and disease. *Acta Neuropathol*. 2017;133:665–704.
- Min S-W, Chen X, Tracy TE, et al. Critical role of acetylation in tau-mediated neurodegeneration and cognitive deficits. *Nat Med*. 2015;21:1154–1162.
- Hutton M, Lendon CL, Rizzu P, et al. Association of missense and 5'-splice-site mutations in tau with the inherited dementia FTDP-17. *Nature*. 1998;393:702–705.
- Harada A, Oguchi K, Okabe S, et al. Altered microtubule organization in small-calibre axons of mice lacking tau protein. *Nature*. 1994;369:488–491.
- Lee VM-Y, Goedert M, Trojanowski JQ. Neurodegenerative tauopathies. *Annu Rev Neurosci*. 2001;24:1121–1159.
- Fitzpatrick AWP, Falcon B, He S, et al. Cryo-EM structures of tau filaments from Alzheimer's disease. *Nature*. 2017;547:185–190.
- Falcon B, Zhang W, Murzin AG, et al. Structures of filaments from Pick's disease reveal a novel tau protein fold. *Nature*. 2018;561:137–140.
- Zhang W, Tarutani A, Newell KL, et al. Novel tau filament fold in corticobasal degeneration. *Nature*. 2020;580:283–287.
- Arakhamia T, Lee CE, Carlomagno Y, et al. Posttranslational modifications mediate the structural diversity of tauopathy strains. *Cell*. 2020;180:633–644.
- Falcon B, Zivanov J, Zhang W, et al. Novel tau filament fold in chronic traumatic encephalopathy encloses hydrophobic molecules. *Nature*. 2019;568:420–423.
- Braak F, Braak H, Mandelkow E-M. A sequence of cytoskeleton changes related to the formation of neurofibrillary tangles and neuropil threads. *Acta Neuropathol*. 1994;87:554–567.
- Grundke-Iqbal I, Iqbal K, Tung YC, Quinlan M, Wisniewski HM, Binder LI. Abnormal phosphorylation of the microtubule-associated protein tau (tau) in Alzheimer cytoskeletal pathology. *Proc Natl Acad Sci U S A*. 1986;83:4913–4917.
- Cohen TJ, Guo JL, Hurtado DE, et al. The acetylation of tau inhibits its function and promotes pathological tau aggregation. *Nat Commun*. 2011;2:252.
- Rizzu P, Van Swieten JC, Joosse M, et al. High prevalence of mutations in the microtubule-associated protein tau in a population study of frontotemporal dementia in The Netherlands. *Am J Hum Genet*. 1999;64:414–421.
- Barghorn S, Zheng-Fischhofer Q, Ackmann M, et al. Structure, microtubule interactions, and paired helical filament

- aggregation by tau mutants of frontotemporal dementias. *Biochemistry*. 2000;39:11714–11721.
29. Gorsky MK, Burnouf S, Dols J, Mandelkow E, Partridge L. Acetylation mimic of lysine 280 exacerbates human Tau neurotoxicity in vivo. *Sci Rep*. 2016;6:22685.
 30. Ajit D, Trzeciakiewicz H, Tseng J-H, et al. A unique tau conformation generated by an acetylation-mimic substitution modulates P301S-dependent tau pathology and hyperphosphorylation. *J Biol Chem*. 2019;294:16698–16711.
 31. Haj-yahya M, Lashuel HA. Protein semisynthesis provides access to tau disease-associated post-translational modifications (PTMs) and paves the way to deciphering the tau PTM code in health and diseased states. *J Am Chem Soc*. 2018;140:6611–6621.
 32. Trzeciakiewicz H, Tseng J-H, Wander CM, et al. A dual pathogenic mechanism links tau acetylation to sporadic tauopathy. *Sci Rep*. 2017;7:44102.
 33. Ramachandran G, Udgaonkar JB. Mechanistic studies unravel the complexity inherent in tau aggregation leading to Alzheimer's disease and the tauopathies. *Biochemistry*. 2013;52:4107–4126.
 34. Ramachandran G, Udgaonkar JB. Evidence for the existence of a secondary pathway for fibril growth during the aggregation of tau. *J Mol Biol*. 2012;421:296–314.
 35. Murzin AG, Falcon B, Crowther RA, et al. Heparin-induced tau filaments are polymorphic and differ from those in Alzheimer's and Pick's diseases. *Elife*. 2019;8:1–24.
 36. Dregni AJ, Mandala VS, Wu H, et al. In vitro 0N4R tau fibrils contain a monomorphic β -sheet core enclosed by dynamically heterogeneous fuzzy coat segments. *Proc Natl Acad Sci U S A*. 2019;116:16357–16366.
 37. Vandenakker CC, Engel MFM, Velikov KP, Bonn M, Koenderink GH. Morphology and persistence length of amyloid fibrils are correlated to peptide molecular structure. *J Am Chem Soc*. 2011;133:18030–18033.
 38. Knowles TP, Fitzpatrick AW, Meehan S, et al. Role of intermolecular forces in defining material properties of protein nanofibrils. *Science*. 2007;318:1900–1903.
 39. Kumar H, Udgaonkar JB. Mechanistic and structural origins of the asymmetric barrier to prion-like cross-seeding between Tau-3R and Tau-4R. *J Mol Biol*. 2018;430:5304–5312.
 40. Harper JD, Lansbury PT. Models of amyloid seeding in Alzheimer's disease and scrapie: Mechanistic truths and physiological consequences of the time-dependent solubility of amyloid proteins. *Annu Rev Biochem*. 1997;66:385–407.
 41. Oosawa F, Asakura S. *Thermodynamics of the polymerization of protein*. London, UK: Academic Press, 1975.
 42. Qiang W, Yau WM, Tycko R. Structural evolution of Iowa mutant β -amyloid fibrils from polymorphic to homogeneous states under repeated seeded growth. *J Am Chem Soc*. 2011;133:4018–4029.
 43. Paravastu AK, Leapman RD, Yau W-M, Tycko R. Molecular structural basis for polymorphism in Alzheimer's β -amyloid fibrils. *Proc Natl Acad Sci U S A*. 2008;105:18349–18354.
 44. Watson MD, Lee JC. N-terminal acetylation affects α -synuclein fibril polymorphism. *Biochemistry*. 2019;58:3630–3633.
 45. Hu Z, Vugmeyster L, Au DF, Ostrovsky D, Sun Y, Qiang W. Molecular structure of an N-terminal phosphorylated β -amyloid fibril. *Proc Natl Acad Sci U S A*. 2019;116:11253–11258.
 46. Cao Q, Boyer DR, Sawaya MR, Ge P, Eisenberg DS. Cryo-EM structures of four polymorphic TDP-43 amyloid cores. *Nat Struct Mol Biol*. 2019;26:619–627.
 47. Boyer DR, Li B, Sun C, et al. The α -synuclein hereditary mutation E46K unlocks a more stable, pathogenic fibril structure. *Proc Natl Acad Sci U S A*. 2020;117:3592–3602.
 48. Kumar H, Singh J, Kumari P, Udgaonkar JB. Modulation of the extent of structural heterogeneity in α -synuclein fibrils by the small molecule thioflavin T. *J Biol Chem*. 2017;292:16891–16903.
 49. Krishnan R, Lindquist SL. Structural insights into a yeast prion illuminate nucleation and strain diversity. *Nature*. 2005;435:765–772.
 50. Chiti F, Stefani M, Taddei N, Ramponi G, Dobson CM. Rationalization of the effects of mutations on peptide and protein aggregation rates. *Nature*. 2003;424:805–808.
 51. Chen D, Drombosky KW, Hou Z, et al. Tau local structure shields an amyloid-forming motif and controls aggregation propensity. *Nat Commun*. 2019;10:2493.
 52. Larini L, Gessel MM, LaPointe NE, et al. Initiation of assembly of tau(273-284) and its Δ K280 mutant: An experimental and computational study. *Phys Chem Chem Phys*. 2013;15:8916–8928.
 53. Shammass SL, Garcia GA, Kumar S, et al. A mechanistic model of tau amyloid aggregation based on direct observation of oligomers. *Nat Commun*. 2015;6:7025.
 54. Horcas I, Fernández R, Gómez-Rodríguez JM, Colchero J, Gómez-Herrero J, Baro AM. WsXM: A software for scanning probe microscopy and a tool for nanotechnology. *Rev Sci Instrum*. 2007;78:013705.
 55. Weis DD, Engen JR, Kass IJ. Semi-automated data processing of hydrogen exchange mass spectra using HX-express. *J Am Soc Mass Spectrom*. 2006;17:1700–1703.
 56. Zhang Z, Smith DL. Determination of amide hydrogen exchange by mass spectrometry: A new tool for protein structure elucidation. *Protein Sci*. 1993;2:522–531.

SUPPORTING INFORMATION

Additional supporting information may be found online in the Supporting Information section at the end of this article.

How to cite this article: Kumar H, Udgaonkar JB. The Lys 280 \rightarrow Gln mutation mimicking disease-linked acetylation of Lys 280 in tau extends the structural core of fibrils and modulates their catalytic properties. *Protein Science*. 2021;1–19. <https://doi.org/10.1002/pro.4030>